Available online at www.sciencedirect.com
ScienceDirect
Journal of Computational Physics 224 (2007) 314–331
JOURNAL OF COMPUTATIONAL PHYSICS
www.elsevier.com/locate/jcp

# A Mach-uniform algorithm: Coupled versus segregated approach

Krista Nerinckx [1], Jan Vierendeels, Erik Dick *

*Ghent University, Department of Flow, Heat and Combustion Mechanics, Sint-Pietersnieuwstraat 41, B-9000 Ghent, Belgium*

Received 1 September 2006; received in revised form 8 February 2007; accepted 13 February 2007
Available online 17 February 2007

**Abstract**

A Mach-uniform algorithm is an algorithm with a good convergence rate for any level of the Mach number. In this paper, the severe time step restriction for low speed flows is removed by treating the acoustic and diffusive terms implicitly. After identification of these terms in the conservative set, we end up with a semi-implicit system. The way to solve this system can be chosen. Three different solution techniques are presented: a fully coupled algorithm, the coupled pressure and temperature correction algorithm [K. Nerinckx, J. Vierendeels, E. Dick, Mach-uniformity through the coupled pressure and temperature correction algorithm, Journal of Computational Physics 206 (2005) 597–623], and a fully segregated pressure-correction algorithm. We analyse the convergence behavior of the considered algorithms for some typical flow problems. Moreover, a Fourier stability analysis is done. For inviscid flow, the fully segregated and the fully coupled algorithm need about as much time steps to reach steady state. Therefore, the more segregation is introduced, the faster the calculation can be done. In case of heat transfer, the fully segregated pressure-correction algorithm suffers from a diffusive time step limit. This is not the case for the semi-segregated coupled pressure and temperature correction algorithm. Finally, when the gravity terms play an important role, only the fully coupled algorithm can avoid an additional time step restriction.


*MSC:* 65N22; 76M12; 76N15; 76R10

*Keywords:* Mach-uniform; Segregated algorithm; Coupled algorithm; Pressure-correction; Fourier analysis; Inviscid flow; Heat transfer; Gravity

## 1. Introduction

Historically, algorithms for CFD have been grouped into two classes: *density-based* methods and *pressure-based* methods. The first class refers to algorithms originally developed for high speed calculations, which treat

* Corresponding author. Tel.: +32 9 264 33 01; fax: +32 9 264 35 86.
*E-mail addresses:* Jan.Vierendeels@UGent.be (J. Vierendeels), Erik.Dick@UGent.be (E. Dick).
[1] Research funded with a fellowship granted by the Flemish Institute for the Promotion of Scientific and Technological Research in the Industry (IWT).

0021-9991/$ - see front matter 
doi:10.1016/j.jcp.2007.02.008

the set of flow equations in a coupled way. The latter class, in which the pressure-correction algorithm [2] is situated, refers to segregated algorithms, originally developed for low speed and incompressible flows. Both types of algorithms have been adapted to make them Mach-uniform, i.e. applicable for all speeds.

With preconditioning, the density-based algorithms were extended towards the low Mach number regime [3,4]. The solution technique is then coupled and time accuracy can only be recovered through an expensive dual time stepping. The other way to obtain a Mach-uniform algorithm is to extend the segregated pressure-correction method towards the high Mach number compressible regime. In the literature, two subclasses can be distinguished, based on how the pressure-correction equation is constructed. In the first class, the pressure-correction equation is derived from the continuity equation [5–11]; in the second class, the energy equation is used for this purpose. As we analysed in [1], deriving the pressure-correction equation from the continuity equation is the right approach for an incompressible and a barotropic fluid. For a perfect gas however, the energy equation should be used, in order to obtain an efficient algorithm. Professor Wesseling and his group were amongst the first to present the latter idea, for adiabatic perfect gas flow (see for example [12–14]).

In this paper, we present the idea that only a classification with regard to the *solution technique* (coupled versus segregated) is valuable: three different types of algorithms are constructed, each of them based on the same principle to reach Mach-uniformity, but applying a different solution technique.

## 2. Semi-implicit system

Mach-uniform efficiency implies a good convergence rate for any level of the Mach number. In [1] we explain how Mach-uniformity can be reached by treating the acoustic and diffusive terms (friction, heat conduction) implicitly. The convective terms, on the other hand, can be treated explicitly. A finite volume method for the two-dimensional Navier–Stokes equations therefore results in the following semi-implicit system

$$\left[\rho_i^{(m+1)}-\rho_i^{[m]}\right]V_i/\Delta t^I+\sum\rho_f^{[m]}w_f^{(m+1)}\,\mathrm{d}s_f=0, \tag{1}$$

$$\left[(\rho u)_i^{(m+1)}-(\rho u)_i^{[m]}\right]V_i/\Delta t^I+\sum(\rho uw)_f^{[m]}\,\mathrm{d}s_f+\sum p_f^{(m+1)}\,\mathrm{d}y_f=\sum(\bar{n}\cdot\vec{\tau}\cdot\bar{1}_x)_f^{(m+1)}\,\mathrm{d}s_f, \tag{2}$$

$$\left[(\rho v)_i^{(m+1)}-(\rho v)_i^{[m]}\right]V_i/\Delta t^I+\sum(\rho vw)_f^{[m]}\,\mathrm{d}s_f+\sum p_f^{(m+1)}\mathrm{d}x_f=\sum(\bar{n}\cdot\vec{\tau}\cdot\bar{1}_y)_f^{(m+1)}\,\mathrm{d}s_f-\rho_i g V_i, \tag{3}$$

$$\left[(\rho E)_i^{(m+1)}-(\rho E)_i^{[m]}\right]V_i/\Delta t^I+\sum(\rho H)_f^{[m]}w_f^{(m+1)}\,\mathrm{d}s_f=\sum(\kappa\nabla T.\bar{n})_f^{(m+1)}\mathrm{d}s_f+\sum(\vec{\tau}\cdot\bar{w})_f^{(m+1)}\cdot\bar{n}\,\mathrm{d}s_f-\rho_i v_i g V_i, \tag{4}$$

with $\rho$ the density, $p$ the pressure, $T$ the temperature, $E$ the specific total energy, $H$ the specific total enthalpy, $\bar{g}=-g\bar{1}_y$ the gravitational acceleration vector, $\vec{\tau}$ the viscous stress tensor, $\kappa$ the heat conduction coefficient and $V_i$ the cell volume. The summation runs over all faces $f$ of the control volume around node $i$. $\mathrm{d}s_f$ is the length of the face $f$ and $w_f$ represents the projection of the velocity vector $\bar{w}=u\bar{1}_x+v\bar{1}_y$ on the outward normal $\bar{n}$ of the face $f$. The equations are given in non-dimensional form. They were non-dimensionalized by choosing three reference quantities for pressure, temperature and length scale, respectively, $\hat{p}_{\mathrm{ref}}$, $\widehat{T}_{\mathrm{ref}}$ and $\widehat{L}_{\mathrm{ref}}$. The hat-sign $\hat{}$ refers to dimensional quantities. Other reference quantities are calculated from these quantities, for example $\hat{\rho}_{\mathrm{ref}}=\rho(\hat{p}_{\mathrm{ref}},\widehat{T}_{\mathrm{ref}})$ with $\rho=\rho(p,T)$ the equation of state, and $\hat{v}_{\mathrm{ref}}=\sqrt{\hat{p}_{\mathrm{ref}}/\hat{\rho}_{\mathrm{ref}}}$.

A multistage time stepping with $k$ stages is used,

$$\begin{aligned}
&Q^{[0]}=Q^n\\
&\vdots\\
&Q^{[m+1]}=Q^{[0]}+\alpha_{m+1}\Delta t\frac{\partial Q^{[m]}}{\partial t}\\
&\vdots\\
&Q^{n+1}=Q^{[k]},
\end{aligned} \tag{5}$$

where $n$ and $n+1$ represent, respectively, the old and the new *time* level, while $[m]$ and $[m+1]$ represent *stage* levels. $Q$ is the state vector $[puvT]^{\mathrm{T}}$ and $\Delta t = t^{n+1} - t^n$ the time step. The slope $\frac{\partial Q^{[m]}}{\partial t}$ is determined as

$$\frac{\partial Q^{[m]}}{\partial t} = \frac{\Delta Q^{[m]}}{\Delta t^I} = \frac{Q^{(m+1)} - Q^{[m]}}{\Delta t^I}, \tag{6}$$

with $Q^{(m+1)}$ some unknown state, $Q^{[m]}$ the known state at level $[m]$, and $\Delta t^I$ a chosen *internal* time step which is only used to define the slope (6). The unknown state $Q^{(m+1)}$ is determined from the semi-implicit systems (1)–(4), in which explicit terms are written at level $[m]$, whereas implicit terms are written at level $(m+1)$. Once $Q^{(m+1)}$ has been solved from the semi-implicit system, we calculate $\Delta Q^{[m]} = Q^{(m+1)} - Q^{[m]}$, and insert it into the multistage time stepping,

$$Q^{[m+1]} = Q^{[0]} + \alpha_{m+1}\Delta t\frac{\Delta Q^{[m]}}{\Delta t^I} = Q^{[0]} + \alpha_{m+1}\omega\Delta Q^{[m]}, \tag{7}$$

with $\omega = \Delta t/\Delta t^I$.

In the convective fluxes, the transported quantities $u, v, H$ are upwinded using a higher order method. Like in [15], we use for the mass flux and the pressure at a face a blending of the high speed AUSM+ flux [16] and a low-speed central flux, $(\rho w)_f = (1-\alpha_f)(\rho w)_f^{\mathrm{AUSM+}} + \alpha_f(\rho w)_f^C + \alpha_f p_{\mathrm{diss}}$, $p_f = (1-\alpha_f)p_f^{\mathrm{AUSM+}} + \alpha_f p_f^C$. A pressure dissipation term $p_{\mathrm{diss}}$ is added to the mass flux to prevent pressure–velocity decoupling at low Mach numbers. $\alpha_f$ is a blending function which varies between 1 for $|Ma_f| < 0.3$ and 0 for $|Ma_f| > 0.5$, with $Ma_f$ the Mach number at the face $f$. The diffusive terms (heat conduction and friction) are discretized centrally.

## 3. Solution technique: coupled versus segregated approach

The way to solve the semi-implicit systems (1)–(4) for the updated values $(m+1)$ can now be chosen: three different solution techniques are considered, varying between a fully coupled and a fully segregated approach.

### 3.1. Fully coupled method

Eqs. (1)–(4) are written in $\Delta$-form, $\Delta(.) = (.)^{(m+1)} - (.)^{[m]}$, and the time derivative terms are expanded with respect to the primitive variables $p, u, v, T$, for example $\Delta\rho = \rho_p\Delta p + \rho_T\Delta T$. The semi-implicit systems (1)–(4) can therefore be written as $[A][\Delta Q] = [B]$, where $[A]$ consists of $(N \times N)$ blocks of size $(4 \times 4)$ (in two-dimensional flow), with $N$ the number of nodes. This $(4N \times 4N)$-system is solved in a coupled way, in each step of the multistage time stepping.

Remark that in the continuity equation (1) and the energy equation (4) the mass flux contains acoustic information, which is treated implicitly. However, only in the low speed part $(\rho w)_f^C$, which is linear, we put the acoustic part $w_f$ at the new level $(m+1)$. The high speed part is defined by the AUSM-interpolation, which is non-linear. A linearization would therefore be necessary to put it at the implicit level. However, the absence of an acoustic time step restriction is only essential for low speed. Therefore, only in the low speed case the acoustic terms have to be treated implicitly. The latter implies that if $|Ma_f| > 0.5$ for all faces $f$, the scheme becomes fully explicit with respect to the acoustic terms. Remark that $\alpha_f$ is defined locally, so that even one cell can have different schemes at its various faces. In the momentum equations, the convective terms are treated explicitly. However, the pressure diffusion term that appears in the low speed part of the mass flux is treated implicitly.

### 3.2. Coupled pressure and temperature correction algorithm

The coupled pressure and temperature algorithm, which finds its place in between the fully coupled and the fully segregated approach, has been presented in [1]. A convective predictor step is followed by an acoustic/diffusive corrector step.

Predictor values (indicated with *) for density and momenta are determined from the continuity and momentum equations, where old values for the pressure are used. Different from [1], the convective terms

are treated explicitly here. Next, corrections for the pressure $p'$ and the temperature $T'$ are determined by solving a system of $(2N \times 2N)$ correction equations. These are derived from the continuity and energy equation. From this, the pressure and temperature can be updated, while the momentum equations are used to update the velocity. We refer to [1] for a detailed explanation. Notice that each stage of (5) consists of a predictor–corrector procedure, so that a $(2N \times 2N)$ system has to be solved in each stage of the multistage time stepping.

### 3.3. Fully segregated method: pressure-correction algorithm

As explained in [1], for a perfect gas flow without heat transfer, a further segregation in the solution procedure is possible. Indeed, the two $(p', T')$-correction equations decouple, and the energy equation becomes a pure pressure-correction equation (without temperature corrections). Therefore, a fully segregated algorithm can be defined, where after the predictor step, pressure corrections are determined from the energy equation. In this fully segregated solution technique, the dimension of the system to be solved in each multistage step is $(N \times N)$ only.

## 4. Fourier stability analysis

The presented algorithms are analysed with the Fourier method. We assume a rectangular grid without stretching and with periodic boundary conditions. The state vector $Q = [p, u, v, T]^{\mathrm{T}}$ is written as the sum of the steady-state solution $\overline{Q}(x, y)$ and an error $\delta Q(x, y, t)$ which is function of the time $t$. For simplicity, we assume a uniform steady-state solution, $\overline{Q}(x, y) = \overline{Q} = \text{constant}$. The error $\delta Q(x, y, t)$ can be written as a sum of Fourier waves with wave number $\omega_x$ in the $x$-direction and wave number $\omega_y$ in the $y$-direction. For example, the pressure is written as

$$p(x, y, t) = \bar{p} + \delta p(x, y, t) = \bar{p} + \phi_p(t)\, \mathrm{e}^{\mathrm{j}(\omega_x x + \omega_y y)}, \tag{8}$$

with j the imaginary unit, and analogously for $u$, $v$, $T$.

We consider two representative flow problems:

- *low Mach number flow*: $\alpha_f = 1$, central discretization for $w_f$ and $p_f$, addition of a pressure dissipation term;
- *high Mach number flow*: $\alpha_f = 0$, upwind discretization for $w_f$ and $p_f$, no pressure dissipation term.

As an example, consider a convective term in the $u$-momentum equation for low speed flow,

$$\left[u_i \rho_i \frac{u_i + u_{i+1}}{2\Delta x}\right]^{[m]} = \left(\bar{u} + \phi_u^m e\right)\left(\bar{\rho} + \phi_\rho^m e\right)\left(2\bar{u} + \phi_u^m e + \phi_u^m e\, \mathrm{e}^{\mathrm{j}\theta_x}\right)\frac{1}{2\Delta x}, \tag{9}$$

with $e = \mathrm{e}^{\mathrm{j}(\omega_x x + \omega_y y)}$, $\phi_\rho = \rho_p \phi_p + \rho_T \phi_T$ and $\theta_x = \omega_x \Delta x$. Products of $\delta$-variables are omitted: only linear perturbations are taken into account. We obtain

$$\frac{1}{\Delta x}\left[\bar{\rho}\bar{u}\bar{u} + \frac{1}{2}\bar{\rho}\bar{u}\phi_u^m(1 + \mathrm{e}^{\mathrm{j}\theta_x})e + \bar{u}\bar{u}\phi_\rho^m e + \bar{\rho}\bar{u}\phi_u^m e\right]. \tag{10}$$

Other terms are treated in a similar way. The factor $e$ and the sum of steady-state terms cancel out in the obtained equation.

Remark that, due to the assumption of a constant background state and the neglect of higher order perturbations, the stability results of the Fourier analysis have to be interpreted as minimum requirements. Therefore, we will add numerical simulations of flow problems to the stability results.

For each of the presented algorithms, the analysis results in a Fourier symbol $F = F(\theta_x, \theta_y, \Delta t', \Delta x, \Delta y, \overline{Q})$, which is defined as $\Delta\Phi^{[m]} = \Phi^{(m+1)} - \Phi^{[m]} = F\Phi^{[m]}$ with $\Phi = [\phi_p, \phi_u, \phi_v, \phi_T]$. The Fourier symbol $F$ is associated with an update $[m]$ to $(m + 1)$ from the semi-implicit system in one stage of the multistage stepping.

For the fully coupled method, the Fourier analysis results in a system of the form $C^d \Delta\Phi = C^m \Phi^{[m]}$, so that $F = C_d^{-1} C_m$. For the predictor–corrector algorithms, separate amplification matrices for the predictor step and for the corrector step are constructed. The predictor step consists of the continuity and momentum equations, and $p^* = p^{[m]}$, leading to a system of the form $P^* \Phi^* = P^m \Phi^{[m]}$. The corrector step consists of the momentum

equations and either the two $p'T'$-equations (coupled pressure and temperature correction algorithm), or the $p'$-equation and $\rho^{(m+1)} = \rho^*$ (pressure correction algorithm). In the corrector step we have $C^{m+1}\Phi^{(m+1)} = C^*\Phi^* + C^m\Phi^{[m]}$. We obtain $F = (C^{(m+1)})^{-1}[C^*(P^*)^{-1}P^m + C^m] - I$, with $I$ the unity matrix.

An update from the semi-implicit system is used in the multistage time stepping (7). We get for an update in time ($n$ to $n+1$) with a $k$ stage stepping $\Phi^{n+1} = G^{MSk}\Phi^n$, with

$$G^{MSk} = I + \alpha_k\omega F + \alpha_k\alpha_{k-1}(\omega F)^2 + \cdots + (\alpha_k\alpha_{k-1}\ldots\alpha_2\alpha_1)(\omega F)^k, \tag{11}$$

where $G^{MSk}$ is the amplification matrix associated with an update in time, $n$ to $n+1$, from the $k$ stage time stepping. It is a function of the Fourier symbol $F$, which is characteristic for the scheme that is used to solve the semi-implicit system in each stage of the stepping.

The time stepping is stable if all eigenvalues of $G^{MSk}$ have a norm smaller than unity. The condition $\|\lambda(G^{MSk})\| = 1$ results in a polynomial equation in $\{Re[\lambda(\omega F)], Im[\lambda(\omega F)]\}$. The solution of the latter is plotted in the $\{Re[\lambda(\omega F)], Im[\lambda(\omega F)]\}$-plane. Furthermore, the eigenvalues $\lambda(\omega F)$ are plotted in the same plane, for a number of combinations $(\theta_x, \theta_y)$, and chosen values for $\overline{Q}$, $\Delta x$, $\Delta y$, $\Delta t^I$ and $\omega$. Remark that the choice of $\Delta t^I$ determines the shape of the eigenvalue curve, while $\omega$ acts as a scaling factor for this curve. In order to obtain a stable time stepping scheme, the eigenvalue curve $\lambda(\omega F(\theta_x, \theta_y))$ should be situated completely within the corresponding $MSk$-time stepping curve.

## 5. Coupled versus segregated approach: behavior in some typical flow problems

We study the behavior of the presented algorithms with regard to three typical flow aspects: inviscid flow, heat transfer and gravity. We focus on stability conditions and convergence behavior. In all simulations a perfect gas is considered.

The used notations concerning the algorithms are given in Table 1. For the exact implementation of all tests, with technical details and remarks, we refer to Appendix A.

### 5.1. Inviscid flow

As a first flow problem, we consider inviscid flow, described by the Euler equations. In order to keep the overview, all results are presented in Table 2 and Fig. 1.

#### 5.1.1. Fourier stability analysis

First, we consider low Mach number flow ($Ma = 0.001$). For the COUP algorithm, $cfl^I$ has to be decreased down to 0.5 to obtain an eigenvalue curve which does not enter the right half plane. Next, the curve can be scaled up with $\omega = 2.7$ before it crosses the time stepping curve. Amongst the segregated algorithms, the PE algorithm can use the highest global CFL number (i.e. $cfl^I * \omega$). For the PT algorithm the global CFL number is somewhat lower. For the PC algorithm the global CFL number is the lowest. This confirms that, for a perfect gas without heat transfer, the corrections should by determined from the energy equation, which imposes the pressure in a direct way for this case [1]. The coupled pressure and temperature algorithm *can* be applied as well, but, due to the influence of the continuity equation in the determination of the corrections,

Table 1
Used notations concerning the algorithms

| | |
|---|---|
| COUP | Fully coupled algorithm |
| PE | Fully segregated pressure-correction algorithm, with pressure corrections form the energy equation |
| PT | Coupled pressure and temperature correction algorithm |
| PC | Fully segregated pressure-correction algorithm, with pressure corrections from the continuity equation (classical approach) |
| U1, U2 | Upwind discretization of first/second-order |
| K3 | Van Leer-$\kappa$ scheme with $\kappa = 1/3$ |
| MS1, MS4, MS5 | Multistage time stepping with 1/4/5 stages (MS4: standard coefficients, MS5: coefficients from [17]) |
| expl, impl | Explicit/implicit convective terms |

Table 2
Inviscid flow: results

| Inviscid flow $M$ | Algorithm | Convective terms | Discretization | $cfl^I$ | $\omega$ | Figure |
|---|---|---|---|---|---|---|
| *Fourier stability analysis* | | | | | | |
| Low ($Ma = 0.001$) | COUP | expl | K3/MS4 | 0.5 | 2.7 | 1a |
| | PE | expl | K3/MS4 | 0.6 | 2.7 | 1b |
| | PT | expl | K3/MS4 | 0.6 | 2.4 | 1c |
| | PC | expl | K3/MS4 | 0.2 | 2.7 | 1d |
| | PE | impl | U1/MS1 | 100 | 1 | 1e |
| | PT | impl | U1/MS1 | 1.1 | 1 | 1f |
| High ($Ma = 2$) | COUP | expl | U2/MS5 | 0.6 | 1.7 | 1g |
| | PE | expl | U2/MS5 | 0.2 | 7.5 | 1h |
| *Test case: inviscid flow past a bump in a channel* | | | | | | |
| Low | COUP | expl | K3/MS4 | 0.7 | 2.2 | 2, 3 |
| | PE | expl | K3/MS4 | 0.7 | 2.9 | 2, 3 |
| | PT | expl | K3/MS4 | 0.7 | 1.9 | 2, 3 |
| | PC | expl | K3/MS4 | 0.5 | 1.8 | 3 |
| High ($Ma = 0.85$) | COUP | expl | minmod/MS5 | 1 | 1.2 | 4a |
| | PE | expl | minmod/MS5 | 0.5 | 5 | 4a |
| | PT | expl | minmod/MS5 | 0.2 | 6 | 4a |
| High ($Ma = 2$) | COUP | expl | minmod/MS5 | 0.7 | 2.1 | 4b |
| | PE | expl | minmod/MS5 | 0.2 | 10 | 4b |
| | PT | expl | minmod/MS5 | 0.1 | 12 | 4b |

it is not optimal. Indeed, the PT algorithm was in fact not developed for this type of flow: only if (enough) heat conduction is present, the PT algorithm is advantageous (see also Section 5.2).

When the convective terms are treated implicitly, the PE algorithm does not suffer from a convective CFL limit: the algorithm is unconditionally stable, at least for small perturbations. For the PT algorithm, however, the CFL number can be taken at most 1.1. In Section 5.2, we will show that its behavior improves considerably in the presence of (enough) heat transfer. For high Mach number flow ($Ma = 2$), $cfl^I$ can be taken at most 0.6 for the fully coupled algorithm. Then, the curve can be scaled up with a factor $\omega = 1.7$. Remark that we calculate the convective CFL number $cfl^I = [u/\Delta x + v/\Delta y]\Delta t$. However, since the scheme becomes explicit in the $x$-direction (see Section 3.1), the stability is in fact determined by $cfl = [(u + c)/\Delta x + v/\Delta y]\Delta t$. For the fully segregated PE algorithm, the internal CFL number has to be taken very low to obtain a good shaped curve: $cfl^I = 0.2$. However, afterwards a large scaling factor can be applied: $\omega = 7.5$.

### 5.1.2. Test case: inviscid flow past a bump in a channel

Each of the presented algorithms only has a time step restriction based on a convective CFL number, since the acoustic and diffusive terms have been treated implicitly. They differ, however, in the cost to solve one time step, since the dimension of the system that has to be solved per multistage step is different. In the fully coupled method this is $(4N \times 4N)$, in the PT algorithm the system is of dimension $(2N \times 2N)$, and in the fully segregated pressure-correction algorithms (PE, PC) this is $(N \times N)$. Hereafter, we will compare their convergence behavior, i.e. the number of time steps needed to reach steady state.

As a numerical test case, we take the inviscid flow past a bump in a channel. First, we focus on very low speed flow. We did simulations for an inlet Mach number $Ma_{\text{in}}$ equal to $10^{-5}$, $10^{-3}$ and $10^{-2}$. In Fig. 2 convergence results are presented. Each plot shows an exact scaling with the Mach number. A Mach-uniform convergence rate is therefore obtained. Table 2 shows the values that could be used for the internal convective CFL number $cfl^I$ and the scaling factor $\omega$ in order to keep the computation stable. First, the maximum value for $cfl^I$ was determined to keep the computation stable with $\omega = 1$. Next, this maximum value for $cfl^I$ was kept constant and $\omega$ was increased as much as possible. The same values hold for the three inlet Mach numbers. The same trends are visible from both the stability analysis and the numerical test cases.

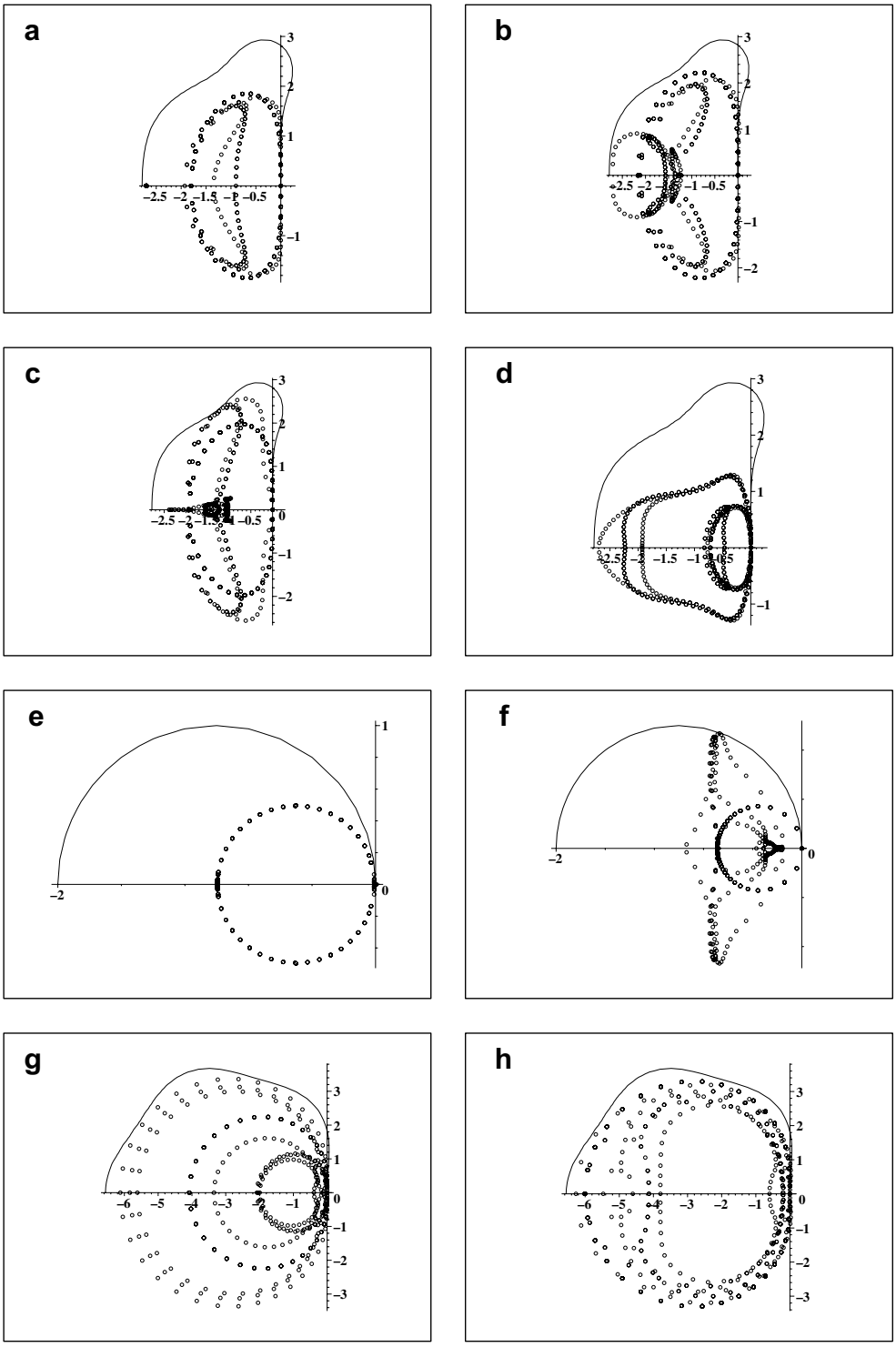


Fig. 1. Inviscid flow: results (see also Table 2).

Fig. 3 compares the convergence plots of the different algorithms for the case $Ma_{in} = 10^{-5}$. For the predictor–corrector algorithms (PE, PT, PC), the PE algorithm converges the fastest: it is the optimal method for the inviscid flow of a perfect gas. The PC algorithm needs the most time to converge, due to the use of the

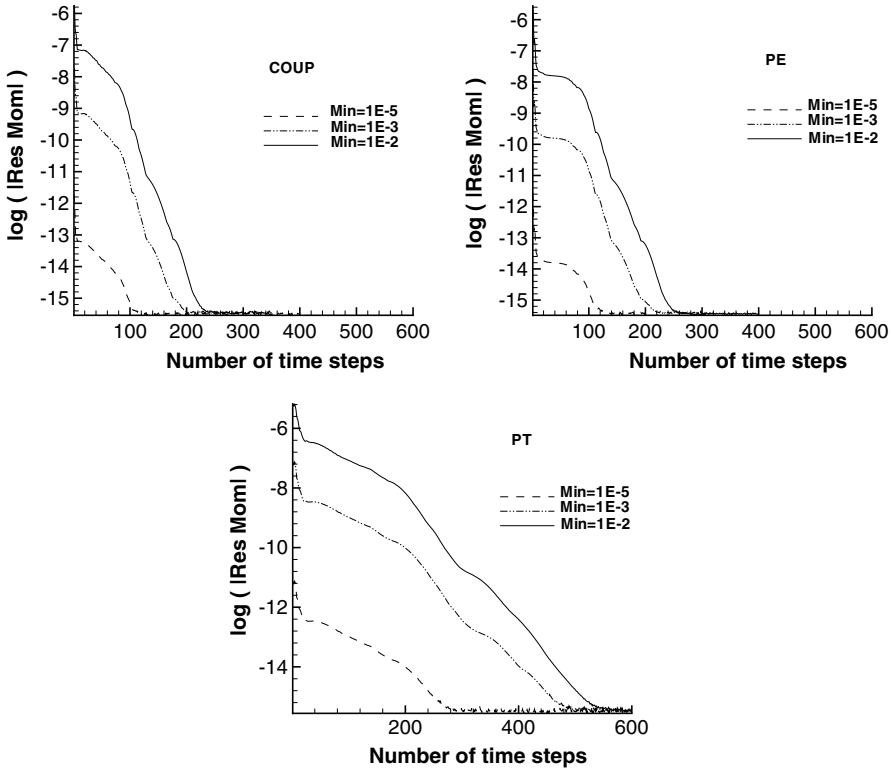


Fig. 2. Channel test case. $\rho v$-momentum residual as a function of the number of time steps.

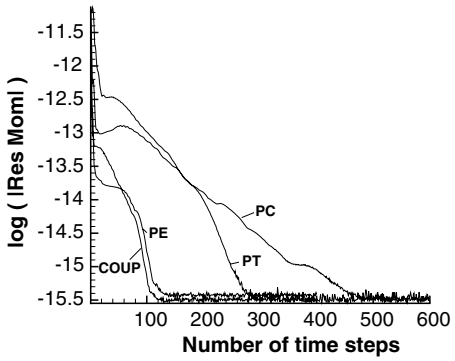


Fig. 3. Channel test case. $Ma_{\text{in}} = 10^{-5}$. $\rho v$-momentum residual as a function of the number of time steps.

continuity equation to determine the pressure (see [1]). The PT algorithm has a convergence rate in between the PE and the PC algorithm. Indeed, due to the influence of the continuity equation in the corrector step, the convergence slows down compared to the PE algorithm. Finally, Fig. 3 shows that the PE algorithm has the same convergence behavior as the fully coupled algorithm. However, the cost to solve one time step is lower for the PE algorithm: only a $(N \times N)$-system has to be solved per time step, opposed to a $(4N \times 4N)$-system for the fully coupled method. Therefore, the more segregation is introduced, the cheaper the simulation can be done. For the case of inviscid flow, complete segregation is possible.

Next, transonic ($Ma_{\text{in}} = 0.85$) and supersonic ($Ma_{\text{in}} = 2$) flow conditions are considered. Table 2 shows the values for the maximum $cfl^I$ and $\omega$. A comparison of the convergence plots is given in Fig. 4. Differently from

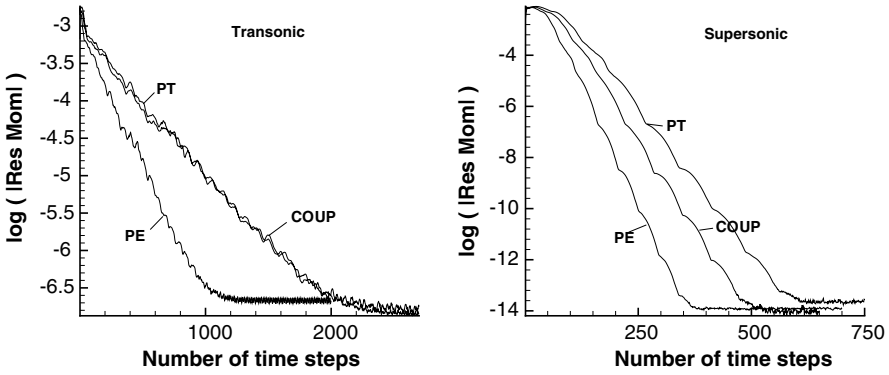


Fig. 4. Channel test case. $\rho v$-momentum residual as a function of the number of time steps. Left: transonic flow, $Ma_{\text{in}} = 0.85$. Right: supersonic flow, $Ma_{\text{in}} = 2$.

the low speed case, the coupled algorithm converges slower than the PE algorithm. Indeed, in the coupled algorithm, only the low speed part of the acoustic terms is treated implicitly, because of the non-linearity of the high speed AUSM+ definition. Therefore, the scheme becomes explicit for faces where $|Ma_f| > 0.5$. This happens for faces (almost) perpendicular to the flow direction, but not for the faces (almost) aligned with the flow direction. The stability for high speed flow is therefore determined by an acoustic CFL number $(u + c)\Delta x/\Delta t$. On the other hand, for the predictor–corrector algorithms, acoustic corrections are introduced in both the $x$ and the $y$ direction. Therefore, the acoustic terms are treated implicitly in both the low speed and the high speed direction. The stability is therefore determined by a convective CFL number. Remark that the CFL numbers given in Table 2 are all convective values, also for the fully coupled algorithm. Finally, Fig. 4 shows that the PT algorithm converges slower than the PE algorithm. This is probably due to the terms in the vertical direction. For that direction, the algorithm behaves as for the low speed case, resulting in a slower convergence for the PT algorithm.

#### 5.1.3. Inviscid flow: conclusion

We conclude that for inviscid flow, complete segregation is possible. The more segregation is introduced, the cheaper the simulation can be done. Therefore, for inviscid flow, the fully segregated algorithm with pressure corrections form the energy equation is the cheapest way to simulate the whole Mach number range.

### 5.2. Heat transfer

For an adiabatic perfect gas flow, the PE algorithm is the cheapest option. When heat conduction is present, however, conductive terms are added in the right-hand side of the pressure-correction equation. They are calculated with $T^*$ values available from the predictor step. This implies that the conductive terms cannot be treated implicitly in this type of algorithm. Therefore, it suffers from a diffusive time step limit. For the coupled pressure and temperature correction algorithm, however, such a limit is absent. The former has already been shown in [1], by means of simulations on a one-dimensional nozzle flow and a thermally driven cavity. We do not repeat these test cases here, and restrict ourselves to the Fourier analysis.

#### 5.2.1. Fourier stability analysis

Results are presented in Table 3 and Fig. 5. $\kappa$ is the heat conduction coefficient and $Ne$ the Von Neumann number. The values of $\kappa$ are chosen at random. We only want to illustrate the effect of the conductive terms on the stability results; no physical problem is modeled here.

For the case of Euler equations, the $cfl^I$ number can be taken 0.7 when the PE algorithm (with explicit convective terms) is used. This $cfl^I$ number is now kept constant, while the value of $\kappa$ is increased. Fig. 5b shows that the algorithm becomes unstable if $\kappa$ is taken too high: if the heat conduction terms become important, they impose the stability condition, and the time step is not determined anymore by the convective CFL number.

Table 3
Heat transfer: results

| Heat transfer<br>Fourier stability analysis (convective terms: expl, discretization: U1/MS1, $\omega = 1$) | | | | | |
|---|---|---|---|---|---|
| *M*-regime | Algorithm | $cfl^I$ | $\kappa$ | *Ne* | Figure |
| Low ($Ma = 0.001$) | PE | 0.7 | 0 | 0 | 5a |
| | | | 0.002 | 0.68 | 5b |
| | PT | 0.5 | 0 | 0 | 5c |
| | | | $10^6$ | $2.4 * 10^8$ | 5d |

*Test case*: nozzle flow, thermally driven cavity (see [1])

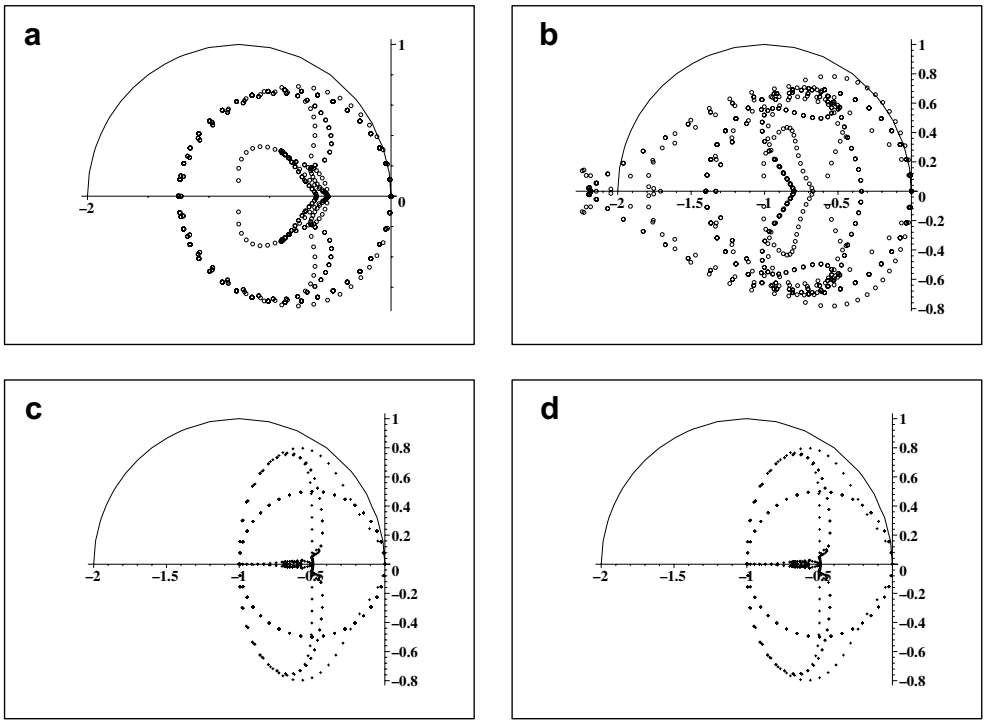


Fig. 5. Heat transfer: results (see also Table 3).

The PT algorithm, however, does not suffer from a diffusive time step limit. The convective CFL number is chosen as the maximum value for the Euler case: $cfl^I = 0.5$. $\kappa$ can be taken infinitely high: there is no diffusive time step limit.

*5.2.2. The coupled pressure and temperature correction algorithm*

Next, we focus on the PT algorithm. Implicit convective terms are used. We already know:

- *Inviscid flow*: the convective CFL number can be taken at most 1.1 (Fig. 1f);
- *Heat transfer*: there is no diffusive time step limit imposed by the conduction terms.

Thus, the PT algorithm is advantageous for those cases where the heat conduction is important. What is more, we will now show that for such a case the behavior of the PT algorithm improves: if the diffusive terms dominate, the convective CFL restriction – present in the inviscid case – is weakened, and even can disappear completely.

To express the relative importance of convective and diffusive stability conditions, we define a cell-Peclet number,

$$Pe = 2\frac{cfl_u}{Ne}, \tag{12}$$

with $cfl_u$ the convective CFL number. With $\Delta x = \Delta y$ and $\alpha$ the thermal diffusivity we have $Ne = \frac{2\alpha\Delta t}{\Delta x^2}$ and $Pe = 2\frac{u\Delta t}{\Delta x}\frac{\Delta x^2}{2\alpha\Delta t} = \frac{u\Delta x}{\alpha}$. Finally, we calculate the time step $\Delta t_{\mathrm{PE}}$, which could be used in the fully segregated pressure-correction algorithm (PE). The latter suffers from a diffusive time step restriction, $Ne \leqslant 1/2$, so that $\Delta t_{\mathrm{PE}} \leqslant \frac{1}{2}\frac{\Delta x^2}{2\alpha}$. The maximum value of the corresponding CFL number is

$$cfl_{u,\mathrm{PE}} = \left(\frac{1}{2}\frac{\Delta x^2}{2\alpha}\right)\frac{u}{\Delta x} = \frac{1}{4}Pe. \tag{13}$$

In the stability analysis of the PT algorithm, several values for $\kappa$ are chosen. The results are given in Table 4. For each case, the highest value of $cfl_u$ is given for which the eigenvalue curve does not cross the first-order time stepping curve. Also the values of $Pe$ and $cfl_{u,\mathrm{PE}}$ are given. The latter does not follow from a stability analysis, but is calculated with (13). The last column indicates the algorithm (either PE or PT) with the highest convective CFL number.

For the case with $Pe = 4.14$, the PE and the PT algorithm give about the same stability restriction. For higher values of $Pe$, it is advantageous to use the fully segregated pressure-correction algorithm, since the restriction imposed by the diffusive terms is not severe. For lower values of $Pe$, the PT algorithm has the weakest restriction, which disappears completely for $Pe = 0.0414$.

### 5.3. Heat transfer: conclusion

We conclude that for flow with heat transfer, the fully segregated algorithm suffers from a diffusive time step limit. The PT algorithm does not suffer from such a limit, and its behavior even improves when (enough) heat transfer is present.

### 5.4. The role of gravity

The gravity terms in the $y$-momentum and the energy equation act as source terms. Therefore, they may introduce an additional time step restriction.

#### 5.4.1. Coupled algorithm versus segregated predictor–corrector algorithm

First, we try to find out how the different type of algorithms – coupled opposed to segregated - behave in the presence of gravity. We add gravity terms to the Euler equations (i.e. viscosity and heat transfer are neglected), and analyse the results of the Fourier stability analysis. This approach allows us to isolate the role of the gravity terms. Results are presented in Table 5 and Fig. 6.

In the fully coupled algorithm, the gravity terms can be treated implicitly without difficulties. For the Euler equations, i.e. $g = 0$, the maximum value of the convective CFL number $cfl_v$ is 0.6 when a first-order upwind discretisation is used for the transported quantities. We take $cfl_v = 0.6$ throughout the analysis and increase the value of $g$ – which represents some non-dimensional number – to see the effect on the plotted eigenvalues. We conclude that, even with an extreme high value for $g$, the fully coupled algorithm remains stable (Fig. 6b).

In a segregated predictor–corrector algorithm, however, it is no longer possible to treat the gravity terms in a fully implicit way. Indeed, consider the $y$-momentum equation of the predictor step. Predictor values $\rho^*$ are

Table 4
PT algorithm: stability results. (convective terms: impl, discretization: U1/MS1, $\omega = 1$, $cfl^l = cfl_u$)

| $M$ | $\kappa$ | $Pe$ | $cfl_u$ | $cfl_{u,\mathrm{PE}}$ | PE or PT |
|---|---|---|---|---|---|
| 0.001 | 0 | $\infty$ | 1.1 | $\infty$ | PE |
| | 0.001 | 4.14 | 2.1 | 1.04 | PT |
| | 0.1 | 0.0414 | $\infty$ | 0.0104 | PT |

Table 5
Gravity: results

| Fourier stability analysis (discretization: U1/MS1, $\omega = 1$, $cfl^I = cfl_v$) | | | | | | | |
|---|---|---|---|---|---|---|---|
| $M$-regime | Algorithm | Conv terms | Grav terms | $cfl_v$ | $g$ | $cfl_g$ | Figure |
| Low ($Ma = 0.001$) | COUP | expl | impl | 0.6 | 0 | | 6a |
| | | expl | impl | 0.6 | $10^6$ | | 6b |
| | PT | impl | expl | 1 | $10^{-7}$ | 0.071 | 6c |
| | | impl | expl | 1 | $10^{-5}$ | 7.1 | 6d |

*Test case: thermally driven cavity (see Section 5.4.2)*

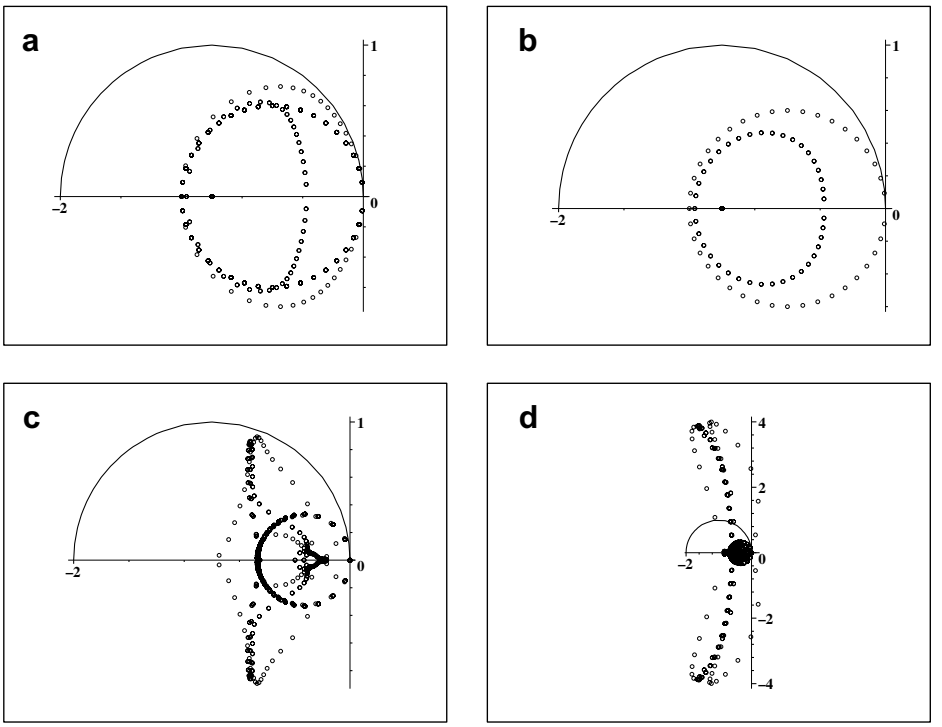


Fig. 6. Gravity: results (see also Table 5).

available from the continuity equation. Those values can be used in the gravity term of the $y$-momentum equation, i.e. $-\rho^* g$ is used in the right-hand side of the latter equation. Since the pressure is frozen in this step ($p^* = p^{[m]}$), only a part of $\rho = \rho(p, T)$ is therefore put at the intermediate level $^*$. Also remark that the introduction of pressure and temperature corrections into $\rho = \rho(p, T)$ would lead to a fully coupled algorithm.

To get insight in the effect of the gravity term, we analyse the eigenvalues of the predictor amplification matrix. We find that the eigenvalues are completely determined by two non-dimensional groups: the convective CFL number $cfl_v$, $cfl_v = \frac{v\Delta t}{\Delta y}$, and a CFL number associated with the gravity force, $cfl_g$,

$$cfl_g = \frac{g\Delta t^2}{\Delta y}. \tag{14}$$

Next, we analyse the stability of the full predictor–corrector scheme as a function of the latter parameter, for the PT algorithm with implicit convective terms. For $g = 10^{-7}$ ($cfl_g = 0.071$) the eigenvalues are situated within the first-order time stepping curve. For $g = 10^{-5}$ ($cfl_g = 7.1$), however, a part of the eigenvalue curve is situated in the right half plane (Fig. 6d).

Remark that the relative importance of the time step restrictions due to $cfl_v$ and $cfl_g$ can be expressed by a cell-Froude number $Fr$. Indeed,

$$\frac{cfl_v}{\sqrt{cfl_g}} = \frac{v\Delta t}{\Delta y}\sqrt{\frac{\Delta y}{g\Delta t^2}} = \frac{v}{\sqrt{g\Delta y}} = Fr. \tag{15}$$

We conclude that a fully coupled algorithm does not suffer from a gravitational time step restriction, if the gravity terms are treated implicitly. For a segregated predictor–corrector algorithm, an additional time step restriction appears. The latter is a consequence of the *segregation*, i.e. the coupling between certain terms is broken up. This can be understood as follows:

Consider the gravity term $-\rho g$ in the right-hand side of the $y$-momentum equation. In a fully coupled algorithm, a perturbation of this term will provoke a response of the pressure: an equilibrium is created between the gravity force and the pressure gradient. In a segregated algorithm, however, the pressure is frozen in the predictor step, and therefore cannot respond directly to the gravity term. Consequently, a disturbance of the velocity field $v$ occurs. In the corrector step, the latter disturbance is transferred to the pressure field. In this way, the pressure responds to the gravity term in an indirect way. In order to prevent that the imbalance in the predictor step between pressure field and gravity force generates an excessively perturbed velocity field, the time step has to be chosen small enough. This explains the time step restriction due to gravity in a segregated algorithm.

### 5.4.2. Test case: thermally driven cavity

As a test case, we take the thermally driven cavity [18], which we also used in [1]. We consider a number of combinations for the Rayleigh number $Ra$ and the non-dimensional temperature difference $\epsilon$. The PT algorithm is used, with implicit convective terms. First, the effect of the gravity terms is studied by means of the Fourier stability analysis. Viscous and heat conduction terms are now taken into account. Afterwards, the results of this analysis are compared with results from a numerical simulation.

### 5.4.3. Fourier stability analysis

Table 6 shows the results of the stability analysis. The values of $Pe$ and $Fr$ are given. As convection dominates in the vertical direction and diffusion in the horizontal direction, $Pe$ is calculated as $Pe = \frac{cfl_v}{Re_x} = \frac{v}{\alpha}\frac{\Delta x^2}{\Delta y}$. A low value of $Pe$ indicates that the diffusive terms are important, a low value of $Fr = v/\sqrt{g\Delta y}$ indicates that the gravity terms are important.

By means of the stability analysis, the maximum allowable time step $\Delta t^I = \Delta t^{\max}$ is determined for which the Fourier symbol does not cross the first-order time stepping curve. Table 6 gives values of $\Delta t^{\max}$ for a number of combinations of $Ra$ and $\epsilon$. First, the analysis is done with $g = 0$. This illustrates whether a time step limit occurs for the case of Navier–Stokes equations, but without influence of the gravity terms. Next, $g$ is given the value as used in the numerical simulation (i.e. calculated from (A.2), see Appendix, Section A.3). This illustrates the effect of the gravity terms on the stability conditions. The two last columns give the corresponding convective CFL number, $cfl_v = v\Delta t/\Delta y$.

For the case $Ra = 10^2$, $\epsilon = 0.6$ we have $Pe \approx O(10^{-3})$, so that the diffusive terms are important. Indeed, for the case $g = 0$ no time step limit occurs. For $g \neq 0$, however, a time step restriction is imposed by the gravity

Table 6
Thermally driven cavity

| $Ra$ | $\epsilon$ | $Pe$ | $Fr$ | $\Delta t_{\max}$ | | $cfl_{v,\max}$ | |
|---|---|---|---|---|---|---|---|
| | | | | $g = 0$ | $g \neq 0$ | $g = 0$ | $g \neq 0$ |
| 1E2 | 0.6 | 0.0024 | 0.23 | $\infty$ | 550000 | $\infty$ | 0.65 |
| 1E2 | 0.01 | 0.0038 | 0.027 | $\infty$ | 45000 | $\infty$ | 0.047 |
| 1E6 | 0.6 | 0.11 | 1.07 | 2400 | 1500 | 1.30 | 0.81 |
| 1E6 | 0.01 | 0.12 | 0.14 | 2500 | 280 | 1.40 | 0.16 |

Results of the Fourier stability analysis.
(PT algorithm, implicit convective terms, U1/MS1, $\omega = 1$).

Table 7
Thermally driven cavity

| $Ra$ | $\epsilon$ | $\Delta t_{max}$, stability analysis, $g \neq 0$ | $\Delta t_{max}$, simulation |
|---|---|---|---|
| 1E2 | 0.6 | 550,000 | 66,000 |
| 1E2 | 0.01 | 45,000 | 52,000 |
| 1E6 | 0.6 | 1500 | 200 |
| 1E6 | 0.01 | 280 | 200 |

Comparison of the stability results following from the Fourier stability analysis and from the numerical simulation of the test case.

terms. When the temperature difference $\epsilon$ decreases ($Ra = 10^2$, $\epsilon = 0.01$), the value of $g$ increases proportional with it (see (A.2)). On the other hand, the velocity level remains the same. This means that $Fr$ diminishes, and the importance of the gravity terms increases. Indeed, for the case $g \neq 0$, a more severe restriction is obtained than for $\epsilon = 0.6$. When the Rayleigh number increases ($Ra = 10^6$, $\epsilon = 0.6$), the velocity level and thus $Pe$ increase: $Pe \approx O(10^{-1})$. This implies that the diffusive terms lose importance. Indeed, for the case $g = 0$, the unconditional stability is lost; a convective CFL number of order 1 is obtained. For $g \neq 0$, this time step restriction remains of the same order, since the importance of the gravity terms is not very pronounced: $Fr \approx O(1)$.

#### 5.4.4. Comparison with results from the numerical simulations

In Table 7, we repeat the $\Delta t_{max}$ values from the stability analysis, for the case $g \neq 0$. The last column gives the maximum time step that could be applied in the numerical simulation of the test case. This time step is fixed during the computation, and the same value is used in the whole domain.

For the cases with $\epsilon = 0.01$, apparently, a good correspondence is obtained. For $\epsilon = 0.6$, the simulation gives a more severe restriction than the stability analysis. This might be due to non-linear effects. Indeed, in the stability analysis, perturbations with respect to a (uniform) steady solution are considered. However, products of perturbations are omitted, which implies that perturbations are small. Therefore, also the changes in the density are assumed to be small. In Section 5.4.1, we have explained the origin of the time step restriction imposed by the gravity terms: when the density changes, an imbalance is created between the gravity force and the pressure gradient. This imbalance should be not too large, so that it can be compensated afterwards in the corrector step. If the stability analysis assumes small density changes, this implies that only small imbalances occur. Thus, the time step restriction following from this analysis is not too severe. In the numerical simulation, however, the assumption of small density changes is only valid for cases with small $\epsilon$.

### 5.5. Gravity: conclusion

We conclude that for a predictor–corrector algorithm, a time step restriction associated with the gravity terms exists. The impact depends on the relative importance with respect to convective and diffusive terms. If the additional time step restriction appears not to be too severe, the predictor–corrector algorithm can be used. Otherwise, the fully coupled approach is the only option.

## 6. Conclusion

We presented a Mach-uniform algorithm, using a semi-implicit approach. Three different solution techniques were considered to solve the semi-implicit system. Naturally, the fully coupled algorithm can do every flow problem without time step restrictions if everything is treated implicitly. However, thinking of the computational cost to solve a large system, this is not beneficial. Indeed, the more segregation can be introduced, the cheaper the calculation can be done. Therefore, the appropriate algorithm has to be chosen depending on the considered application. We conclude for a perfect gas flow:

- Inviscid flow (Euler) : the fully segregated algorithm with pressure corrections form the energy equation is the cheapest way to simulate the whole Mach number range;

- Heat conduction: if a diffusive time step limit does not harm, the fully segregated algorithm still can be applied. Otherwise the coupled pressure and temperature algorithm can be used;
- Gravity: if the time step restriction due to the gravity terms is not too severe (i.e. the gravity does not really dominate the other terms), one of the predictor–corrector algorithms can be applied. Otherwise, the fully coupled method is the only option.

## Appendix A. Results: technical details and remarks

### A.1. Inviscid flow

#### A.1.1. Fourier stability analysis (Section 5.1.1)

We consider a Cartesian grid, uniformly spaced, with $\Delta x = \Delta y = 1$. The flow is aligned with the grid ($v = 0$), the horizontal velocity component $u$ is calculated from a chosen Mach number $Ma$. We take $p = 1$, $T = 1$ and $\theta_{x,y} = 2\pi i_{x,y}/N_{x,y}$ with $i_{x,y} = [0, 1, \ldots, N_{x,y} - 1]$, $N_x = 40$, $N_y = 4$. The time step $\Delta t^I$ is calculated from a chosen convective CFL number, $\Delta t^I = cfl^I \Delta x/u$ and the scaling factor $\omega$ is chosen.

#### A.1.2. Test case: inviscid flow past a bump in a channel (Section 5.1.2)

The grid has $48 \times 16$ cells. In each stage of the multistage stepping, the updates obtained from the semi-implicit system are multiplied with a factor $\omega$ before they are inserted in the time stepping. The time step used in the semi-implicit system is derived from a chosen convective CFL number $cfl^I$,

$$\Delta t^I = \frac{cfl^I}{\max_{i,j}\left[\frac{|w\,\mathrm{d}s|_{fr}+|w\,\mathrm{d}s|_{fu}}{V_{ij}}\right]}, \tag{A.1}$$

with $V_{ij}$ the volume of the cell around node $(i, j)$, $fr$ the right cell face and $fu$ the upper cell face. The time step value is calculated at the beginning of each time step. It is kept constant during the stages of the multistage stepping, and the same value is used for all cells (though a local time stepping could be used as well).

In each of the convergence plots, we consider the flux balance $\sum[(\rho v w)_f \,\mathrm{d}s_f + p_f \,\mathrm{d}x_f]$ of the $(\rho v)$-momentum equation. The shown residual is the L1-norm of the vector composed of the $(\rho v)$-flux balances for each cell. The other equations (continuity, $(\rho u)$-momentum, and energy) have a similar convergence behavior; the $(\rho v)$-momentum equation needs the most time steps to converge.

We stress that we only want to compare the convergence behavior of the presented algorithms. A lot of aspects can be optimized, but this can be done for each method in the same manner. Firstly, a fixed time step for all cells is used. In a steady-state problem, this can be altered to local time stepping, i.e. stepping with the highest allowable time step for each cell. Secondly, we used a direct solver for the system in each multistage step. This is of course very costly, but does not influence a comparison of the number of time steps to steady state. More optimized solvers, like iterative methods or multigrid, should be used in practice. In the choice of such a solver, the structure of the considered system should be taken into account. Remark that also the multistage stepping as a whole can be inserted in a multigrid procedure. Finally, also the implementation of the boundary conditions is quite primitive. At the inlet total pressure, total temperature and horizontal flow direction are imposed, while the Mach number is extrapolated; at the outlet the Mach number is imposed and total pressure, total temperature and flow direction are extrapolated. Such boundary conditions are very reflective. This will influence the convergence results in some cases, but, again, this happens for each of the considered methods, so that an honest comparison is still possible. Because of the presence of a shock in the high Mach number cases, a limiter (minmod) is used. For the time stepping, the five stage scheme of [17] with coefficients $\{0.066, 0.16, 0.307, 0.576, 1\}$ is used. Remark that for the transonic case, the number of time steps needed to reach steady state is much larger than for the low speed flows. The stiffness at the sonic point is a possible explanation of this behavior. Also the boundary conditions can cause this slowdown, because of their reflective character. The premature off-leveling of the residuals in the transonic case, is caused by fluctuations of the minmod-limiter in the presence of the (normal) shock. It can be remedied by freezing the limiter after some orders of convergence.

### A.2. Heat transfer

#### A.2.1. Fourier stability analysis (Section 5.2.1)

Heat conduction is present in both the $x$ and $y$ direction. The Von Neumann number reads $Ne = \alpha\Delta t\left(\frac{1}{\Delta x^2}+\frac{1}{\Delta y^2}\right)$, with $\alpha = \kappa/(\rho c_p)$ the thermal diffusivity. We take $\Delta x = \Delta y = 1$, $p = T = 1$ and $v = 0$. The time step is calculated from a chosen convective CFL number $cfl^I$. The heat conduction terms are added to the Euler equations, i.e. viscosity and gravity are omitted.

#### A.2.2. The coupled pressure and temperature correction algorithm (Section 5.2.2)

We take $\mu = 0$ and $v = 0$, but heat conduction is present in both the $x$ and $y$ direction. The velocity $u$ is calculated from a chosen Mach number $Ma$ and we take $\Delta x = \Delta y$ and $p = T = 1$. The time step is calculated from a chosen convective CFL number $cfl_u$.

### A.3. The role of gravity

#### A.3.1. Coupled algorithm versus segregated predictor–corrector algorithm (Section 5.4.1)

The horizontal velocity component is taken zero ($u = 0$), and the vertical component $v$ is calculated from the given Mach number. We take $\Delta y = \Delta x = 1$, $u = 0$ and the time step is derived from a chosen convective CFL number.

#### A.3.2. Thermally driven cavity (Section 5.4.2)

This test case concerns a squared cavity of dimension $L \times L$ filled with a perfect gas. The upper and lower walls are isolated (adiabatic). The left-hand side is heated (temperature $T_h$) and the right-hand side is cooled (temperature $T_c$), which causes a very slow circular movement of the gas due to natural convection. The driving force is expressed by the Rayleigh number,

$$Ra = Pr\frac{\hat{g}\hat{\rho}_{\mathrm{ref}}^2(2\epsilon)\widehat{L}^3}{\left[\hat{\mu}(\widehat{T}_{\mathrm{ref}})\right]^2}, \quad \text{with } \epsilon = \frac{\widehat{T}_h - \widehat{T}_c}{2\widehat{T}_{\mathrm{ref}}} \tag{A.2}$$

the non-dimensional temperature difference and $Pr$ the Prandl number. The hat refers to dimensional quantities. Chosen reference values are $\hat{p}_{\mathrm{ref}} = 101,325$ Pa, $\widehat{T}_{\mathrm{ref}} = 600$ K and $\widehat{L}_{\mathrm{ref}} = \widehat{L} = 1$ m.

All technical details concerning this test case can be found in [19,20] or [1]. The dynamic viscosity $\hat{\mu} = \hat{\mu}(\widehat{T})$ is given by Sutherland's law and is non-dimensionalised using the reference value $\hat{\mu}_{\mathrm{ref}} = \hat{\rho}_{\mathrm{ref}}\hat{v}_{\mathrm{ref}}\widehat{L}_{\mathrm{ref}}$. The Prandl number $Pr$ is assumed to remain constant, equal to 0.71. The heat conduction coefficient is calculated as $\kappa = c_p\mu/Pr$. The non-dimensional value for $g$ is determined as $g = \hat{g}\widehat{L}_{\mathrm{ref}}/\hat{v}_{\mathrm{ref}}^2$ and $\hat{g}$ is calculated from the Rayleigh number (A.2).

#### A.3.3. Fourier stability analysis

In the stability analysis the following parameters are used:

- Positions are given in non-dimensional coordinates. $y = 0$ represents the bottom of the cavity, $y = 1$ is the upper wall, $x = 0$ is the left (hot) wall, and $x = 1$ is the right (cold) wall. The analysis is done for the point A where the vertical velocity $v$ has its maximum size. It is found at half height ($y_A = 0.5$) and close to the cold wall. The position $x_A$ depends on the considered case $(Ra, \epsilon)$ and is given in Table A.1.

Table A.1
Thermally driven cavity

| $Ra$ | $\epsilon$ | $\bar{p}$ | $x_A$ | $\Delta x$ | $\Delta y$ | $\lvert u\rvert$ | $\lvert v\rvert$ |
|---|---|---|---|---|---|---|---|
| 1E2 | 0.6 | 0.95736 | 0.903 | 0.0142 | 0.067 | 5.79E − 10 | 7.93E − 8 |
| 1E2 | 0.01 | 0.99999 | 0.818 | 0.0247 | 0.067 | 5.27E − 10 | 6.97E − 8 |
| 1E6 | 0.6 | 0.92449 | 0.976 | 0.00455 | 0.067 | 1.33E − 7 | 3.63E − 5 |
| 1E6 | 0.01 | 0.99998 | 0.963 | 0.00607 | 0.067 | 1.03E − 6 | 3.76E − 5 |

Parameters used in the Fourier stability analysis.

- The corresponding grid dimensions are given in Table A.1, and are determined from the grid that was used in the numerical simulation of the test case (stretched grid).
- Table A.1 also gives the (non-dimensional) velocity components. They were determined from a converged solution. Only positive velocity values are used in the stability analysis.
- The pressure is taken as $\bar{p}$, which is the mean pressure in the cavity. The values were taken from [19] and are given in Table A.1. The temperature is taken as $T_A \approx 1 - \epsilon/2$.
- The analysis is done for a first-order upwind discretisation of the transported quantities. The scaling factor $\omega$ is taken unity.

*A.3.4. Comparison with results from the numerical simulations*

All the numerical simulations of the test case are done with a first-order upwind discretisation and a first-order time stepping. A stretched grid with $65 \times 65$ nodes and a maximum aspect ratio of 80 is used. Remark that this is quite a coarse grid. However, it is not our goal to illustrate accuracy here; the tests are only used to illustrate stability conditions. The initial state is taken as zero velocities, a hydrostatic pressure field, and a linearly varying temperature field between the hot and the cold wall.

Finally some remarks:

- A measure to weaken the stability condition imposed by the gravity terms, is to start from a better initial state, for example from a converged solution at a Rayleigh number that is one order lower. Another possibility is to increase the time step once some orders of convergence are obtained.
- The linear stability analysis showed that the fully coupled algorithm does not suffer from a gravitational stability restriction. However, non-linear effects, which are not visible in the stability analysis, may cause stability problems in the first, non-linear part of the convergence. Also for a fully coupled algorithm, the start from a good initial state can therefore be of great importance.

## References

[1] K. Nerinckx, J. Vierendeels, E. Dick, Mach-uniformity through the coupled pressure and temperature correction algorithm, Journal of Computational Physics 206 (2005) 597–623.
[2] S.V. Patankar, D.B. Spalding, A calculation procedure for heat, mass and momentum transfer in three-dimensional parabolic flows, International Journal of Heat and Mass Transfer 15 (1972) 1787–1806.
[3] E. Turkel, Preconditioned methods for solving the incompressible and low speed compressible equations, Journal of Computational Physics 72 (2) (1987) 277–298.
[4] J.M. Weiss, W.A. Smith, Preconditioning applied to variable and constant density flows, AIAA Journal 33 (11) (1995) 2050–2057.
[5] I. Demirdžić, Ž Lilek, M. Perić, A collocated finite volume method for predicting flows at all speeds, International Journal for Numerical Methods in Fluids 16 (1993) 1029–1050.
[6] P. Batten, F.S. Lien, M.A. Leschziner, A positivity-preserving pressure-correction method, in: Proceedings of the 15th International Conference on Numerical Methods in Fluid Dynamics, Lecture Notes in Physics, vol. 490, Springer, 1996, pp. 148–151.
[7] W. Shyy, S.S. Thakur, H. Ouyang, J. Liu, E. Blosch, Computational Techniques for Complex Transport Phenomena, Cambridge University Press, 1997.
[8] R.I. Issa, M.H. Javareshkian, Pressure-based compressible calculation method utilizing total variation diminishing schemes, AIAA Journal 36 (9) (1998) 1652–1657.
[9] H. Bijl, P. Wesseling, A unified method for computing incompressible and compressible flows in boundary-fitted coordinates, Journal of Computational Physics 141 (1998) 153–173.
[10] F. Moukalled, M. Darwish, A high-resolution pressure-based algorithm for fluid flow at all speeds, Journal of Computational Physics 168 (2001) 101–133.
[11] K. Nerinckx, J. Vierendeels, E. Dick, A Mach-uniform pressure correction algorithm with AUSM+ flux definitions, International Journal of Numerical Methods in Heat & Fluid Flow 16 (6) (2006).
[12] P. Wesseling, D.R van der Heul, C. Vuik, Unified methods for computing compressible and incompressible flows, in: Proceedings of ECCOMAS 2000, Barcelona, 11–14 September 2000.
[13] I. Wenneker, A. Segal, P. Wesseling, A mach-uniform unstructured staggered grid method, International Journal for Numerical Methods in Fluids 40 (2002) 1209–1235.
[14] D.R. Van der Heul, C. Vuik, P. Wesseling, A conservative pressure correction method for flow at all speeds, Computers & Fluids 32 (2003) 1113–1132.

[15] J. Vierendeels, B. Merci, E. Dick, Blended AUSM+ method for all speeds and all grid aspect ratios, AIAA Journal 39 (12) (2001) 2278–2282.
[16] M.-S. Liou, Mass flux schemes and connection to shock instability, Journal of Computational Physics 160 (2000) 623–648.
[17] E. Dick, C. Riemslagh, Multi-staging of Jacobi relaxation in multigrid methods for steady euler equations, II, Journal of Computational and Applied Mathematics 59 (1995) 339–348.
[18] D. R Chenoweth, S. Paolucci, Natural convection in an enclosed vertical air layer with large horizontal temperature differences, J. Fluid Mech. 169 (1986) 173–210.
[19] J. Vierendeels, B. Merci, E. Dick, Benchmark solutions for the natural convective heat transfer problem in a square cavity with large horizontal temperature differences, International Journal of Numerical Methods for Heat and Fluid Flow 13 (8) (2003) 1057–1078.
[20] J. Vierendeels, B. Merci, E. Dick, A multigrid method for natural convective heat transfer with large temperature differences, Journal of Computational and Applied Mathematics 168 (2004) 509–517.